Edinburgh Research Explorer

Functional Analysis of RNA Structures Present at the 3 ' Extremity of the Murine Norovirus Genome: the Variable Polypyrimidine Tract Plays a Role in Viral Virulence

Vol. 84, No. 6

Functional Analysis of RNA Structures Present at the 3′ Extremity of the Murine Norovirus Genome: the Variable Polypyrimidine Tract Plays a Role in Viral Virulence[▽][†]

Dalan Bailey,[1][‡] Ioannis Karakasiliotis,[1][‡][§] Surender Vashist,[1] Liliane Man Wah Chung,[1] Jivan Reese,[1] Nora McFadden,[1] Alicia Benson,[2] Felix Yarovinsky,[2] Peter Simmonds,[3] and Ian Goodfellow[1]*

Calicivirus Research Group, Department of Virology, Faculty of Medicine, Imperial College London, Norfolk Place, London W2 1PG, United Kingdom[1]; UT Southwestern Medical Center at Dallas, 5323 Harry Hines Blvd., Dallas, Texas 75390-9093[2]; and Centre for Infectious Diseases, University of Edinburgh, Summerhall, Edinburgh EH9 1QH, United Kingdom[3]

Interactions of host cell factors with RNA sequences and structures in the genomes of positive-strand RNA viruses play various roles in the life cycles of these viruses. Our understanding of the functional RNA elements present in norovirus genomes to date has been limited largely to *in vitro* analysis. However, we recently used reverse genetics to identify evolutionarily conserved RNA structures and sequences required for norovirus replication. We have now undertaken a more detailed analysis of RNA structures present at the 3′ extremity of the murine norovirus (MNV) genome. Biochemical data indicate the presence of three stable stem-loops, including two in the untranslated region, and a single-stranded polypyrimidine tract [p(Y)] of variable length between MNV isolates, within the terminal stem-loop structure. The well-characterized host cell pyrimidine binding proteins PTB and PCBP bound the 3′-untranslated region via an interaction with this variable sequence. Viruses lacking the p(Y) tract were viable both in cell culture and upon mouse infection, demonstrating that this interaction was not essential for virus replication. However, competition analysis with wild-type MNV in cell culture indicated that the loss of the p(Y) tract was associated with a fitness cost. Furthermore, a p(Y)-deleted mutant showed a reduction in virulence in the STAT1^{−/−} mouse model, highlighting the role of RNA structures in norovirus pathogenesis. This work highlights how, like with other positive-strand RNA viruses, RNA structures present at the termini of the norovirus genome play important roles in virus replication and virulence.

Noroviruses are now well established as the leading cause of nonbacterial gastroenteritis in the developed world (reviewed in references 31 and 34), but recent studies have also demonstrated links with more significant clinical disease, e.g., exacerbation of inflammatory bowel disease (20), an outbreak of necrotizing enterocolitis (41), and the induction of seizures in neonates (8). The understanding of norovirus translation, replication, and virulence has lagged behind that for other viruses due to the inability to propagate human noroviruses efficiently in tissue culture. Recent advances in the field have led to the generation of norovirus replicons (5, 6), the demonstration that human norovirus RNA is infectious in tissue culture (13), and an unconfirmed report that a highly differentiated cell culture system can be infected with human noroviruses (38). Although many caliciviruses have been used as models for the study of human noroviruses (reviewed in reference 42), the identification of murine norovirus (MNV) in 2003 (19) led to unprecedented advances in the analysis of many aspects of

norovirus biology, as to date this is the only norovirus which replicates efficiently in tissue culture. In addition, the recent development of reverse genetic systems for murine norovirus (7, 44) has allowed the identification of a virulence determinant in the major capsid protein (1) and the first identification of functional RNA sequences/structures in the norovirus genome (35).

The murine norovirus genome carries four potential open reading frames (ORFs) (Fig. 1A). ORF1 encodes a large polyprotein which is posttranslationally cleaved by the virus-encoded protease (NS6) into several proteins which are involved in various aspects of genome replication (37). ORF2 and ORF3 code for the major and minor capsid proteins VP1 and VP2, respectively. In addition, the MNV genome is also known to contain a fourth potential ORF (Fig. 1A) (ORF4), which is highly conserved between numerous strains (40) and whose expression and function have yet to be examined.

Due to the limited coding capacity of their genomes, small positive-strand RNA viruses rely heavily on host cell nucleic acid binding proteins for efficient genome translation and replication (reviewed in reference 22). These host cell factors often play many roles in the virus life cycle by interacting with specific RNA sequences and/or structures present within the viral genome. Such factors are also a major determinant of viral tropism, as their relative expression levels may determine the efficiency with which a virus can replicate in a particular tissue and, as a result, cause disease. Previous work with human norovirus has identified several host factors interacting

FIG. 1. The murine norovirus genome contains three 3′-terminal stem-loop RNA structures. (A) Schematic representation of murine norovirus genome, highlighting the four predicted open reading frames and the mature replicase proteins produced from ORF1. (B) Predicted RNA secondary structure of the 3′ end of the MNV genome. The positions of the RNase cleavage sites, as determined by limited RNase digestion followed by primer extension, are highlighted on the bioinformatically predicted structure for the MNV 3′ end. The genetic sequence variation of 38 published murine norovirus 3′-end sequences is also provided, highlighting those bases which either are invariant, show signs of covariation, vary but maintain base pairing, or vary without maintaining base pairing. ClustalW analysis was performed using all available murine norovirus

with the 5′ and 3′ ends of the viral genome (15, 16). Although a recent study clearly indicated that some cellular factors are potentially involved in norovirus genome circularization (32), the identities of these and the functions of the known binding proteins have yet to be determined.

Our previous studies using computational analysis resulted in the identification of several highly conserved RNA structures at various positions in the MNV genome (35). Furthermore, preliminary analysis using reverse genetics demonstrated that these RNA structures played an important role in unknown aspects of the MNV life cycle. We have now extended this analysis to perform a more detailed characterization of the RNA structures present at the 3′ end of the MNV genome, identifying sequences and structures important for replication in tissue culture. We have also demonstrated that a polypyrimidine-rich [p(Y)] tract, present as a single-stranded terminal loop, is nonessential for virus replication in tissue culture but contributes to virulence in the STAT1$^{-/-}$ mouse model of MNV pathogenesis. This is the first report of RNA structures playing a role in the virulence of any member of the *Caliciviridae* family.

MATERIALS AND METHODS

Cells and antibodies. Murine macrophage RAW 264.7 cells and baby hamster kidney cells expressing T7 polymerase (BSR-T7 cells) (3) were maintained at 37°C and 10% CO$_2$ in Dulbecco's modified Eagle's medium (DMEM) containing 10% fetal calf serum and an antibiotic cocktail of penicillin (100 SI units/ml) and streptomycin (100 μg/ml). Bone-derived macrophages (BMMs) from BALB/c mice were isolated from the thigh bone, differentiated, and maintained as detailed previously (27). Rabbit polyclonal antibodies against the MNV NS7 polymerase and capsid protein were developed in the laboratory (7) and obtained from Herbert Virgin (Washington University in St. Louis), respectively.

Protein expression and purification. For the purification of glutathione *S*-transferase–PTB (GST-PTB), *Escherichia coli* DH5α cells were transformed with the pGEX6P-1 PTB plasmid, provided by Richard Jackson (University of Cambridge, United Kingdom). Cells from a single colony were grown in LB at 37°C to an optical density at 600 nm (OD$_{600}$) of 0.6. Isopropyl-β-D-thiogalactopyranoside (IPTG) was added at a final concentration of 0.1 mM, and protein expression was induced for 2 h. The cells were lysed using a French press under high pressure (10^8 Pa) in phosphate-buffered saline (PBS) containing 0.5 mM dithiothreitol (DTT), 10 mM EDTA, 3 μg/ml leupeptin and pepstatin, 1% Triton X-100, and 1 mM phenylmethylsulfonyl fluoride (PMSF). The clarified lysate was passed through a glutathione-Sepharose column and washed with PBS containing 0.5 mM DTT, 10 mM EDTA, and 1% Triton X-100. A second wash with 50 mM Tris, pH 8.0, 150 mM NaCl, and 0.5 mM DTT followed. The protein was then eluted in 10 mM reduced glutathione, 50 mM Tris, pH 8.0, 150 mM NaCl, and 0.5 mM DTT and dialyzed against 50 mM HEPES, pH 7.6, 1 mM DTT, 1 mM MgCl$_2$, and 20% glycerol. His-PCBP was purified by transformation of *E. coli* JM109 cells with the pQE30:PCBP1 and pQE:PCBP2 plasmids for His-PCBP1 and His-PCBP2, respectively (kindly provided by Bert Semler, University of California, Irvine). Cells from a single colony were grown in LB at 37°C to an OD$_{600}$ of 0.6. IPTG was added at a final concentration of 0.1 mM, and protein expression was induced for 2 h. For His-PCBP1 and His-PCBP2, the cells were pelleted and resuspended in lysis buffer (50 mM Tris, pH 8.0, 20% glycerol, 500 mM NaCl) containing lysozyme (1 mg/ml). The cells were incubated on ice for 30 min and sonicated for complete lysis. Protein purification was performed using Ni-nitrilotriacetic acid (Ni-NTA; Qiagen) according to the manufacturer's instructions. His-PCBP1 and His-PCBP2 preparations were dialyzed against 50 mM Tris, pH 7.5, 100 mM KCl, 1 mM DTT, 0.05 mM EDTA, and 5% glycerol. All proteins were stored at −80°C until required, and the protein concentration was determined using the BCA assay (Pierce).

Plasmid constructs. The construction of the wild-type MNV cDNA constructs [wild type and wild type (v)] was described previously (1, 7), as was that of SL3 ssm (described as m54 in reference 35). Clones ΔSL2 GA, ΔSL3, ΔSL2+3, SL3 ssm R, SL3 GNRA, SL3 GNRA (v), and SL3 AAAA were generated by overlap mutagenic PCR (primer details are available upon request), using KOD Hi-Fidelity *Taq* polymerase (Merck Biosciences).

Virus recovery by reverse genetics. Virus recovery using reverse genetics was performed using BSR-T7 cells for transfection and RAW 264.7 cells for virus titration, as described in detail previously (7). Briefly, 1 μg of full-length viral cDNA clone (e.g., SL3 ssm R) was transfected, using the Lipofectamine 2000 transfection reagent (Invitrogen), into BSR-T7 cells previously infected with a recombinant fowlpox virus expressing T7 RNA polymerase at a multiplicity of infection (MOI) of approximately 0.5. After 24 h, cells were freeze-thawed (at −80°C) to release virus particles. The thawed lysate was clarified and filtered (0.22-μm filter) before 50% tissue culture infective dose (TCID$_{50}$) titrations were undertaken with RAW 264.7 cells. The viral TCID$_{50}$ was determined by visual inspection of the cell cultures at 5 days postinfection. Stocks of high-titer passage 1 virus for experimentation were generated by infecting a 60% monolayer of RAW cells at an MOI of 0.01. Virus was similarly extracted, but at 48 h postinfection. Viruses for *in vivo* experimentation were further concentrated by ultracentrifugation at 100,000 × *g* for 4 h prior to resuspension in tissue culture media. The correct sequences of all viruses generated during this study were confirmed by sequencing of viral RNA from infected cells prior to use.

RNA structure probing and footprinting analysis. RNA structure probing was performed using RNases V1, A, T1 (Ambion), and T2 (MoBiTec GmbH). A total of 1 μg of *in vitro*-transcribed, gel-purified, and refolded RNA (65°C for 10 min followed by cooling to room temperature) was mixed with yeast RNA and structure buffer provided with the RNases (Ambion). Digestions were performed at 30°C for 10 min with appropriate enzyme concentrations to allow single-hit kinetics. The reactions were stopped using inactivation/precipitation buffer, RNA precipitated, and subsequently washed with 70% ethanol and resuspended in 10 μl of nuclease-free water. Two microliters of this RNA was used for primer extension, using end-labeled primers and avian myeloblastosis virus (AMV) reverse transcriptase as described by the manufacturer (Promega). A sequencing ladder generated using the same primer was run along with the primer extension products in a 7 M urea–6% acrylamide sequencing gel. The gel was dried, and the radioactive signal was monitored using a phosphorimager.

For RNA footprinting analysis, RNA was incubated with a 10-fold molar excess of protein (GST-PTB, GST, or His-PCBP2) for 15 min prior to subsequent RNase digestions and primer extensions, performed as described above. Protein storage buffer (see above for further details) or GST protein was used to control for any nonspecific effects on the primer extension reaction.

EMSAs. All radioactive probes were generated by *in vitro* transcription of PCR products containing the region of interest under the control of a T7 RNA polymerase promoter in the presence of ^{32}P-labeled UTP. All RNA probes were gel purified using urea-PAGE. Radioactively labeled RNA was excised, eluted, and precipitated prior to quantification by spectrophotometry. RNA was refolded by heat denaturation followed by slow annealing (~1°C/min) prior to use. The 7.5-μl electrophoretic mobility assay (EMSA) reaction mixtures contained 85 nM radioactive RNA probe, GST-PTB or His-PCBP2 at various concentrations (see figures for more details), 0.67 μg/μl yeast tRNA (Ambion), 50 mM HEPES, pH 7.6, 25 mM KCl, 2.5 mM MgCl$_2$, 1 mM DTT, and 4% glycerol. All reaction mixtures were incubated for 10 min at 30°C, and the mixtures were separated in a 4% acrylamide gel (acrylamide:bis-acrylamide, 19:1) containing 5% glycerol. The EMSA gels were dried and visualized on a phosphorimager screen. Band quantification was performed using the ImageQuant 5.0 software package (Molecular Dynamics).

Analysis of viral growth kinetics. Growth curves were performed to assess the single and multistep growth kinetics for the wild-type, wild-type (v), SL3 GNRA, and SL3 GNRA (v) viruses. Single-step growth curves were performed using an

---

sequences in the NCBI database (details available on request). The stop codon of the VP2 coding sequence in SL1 is also highlighted. (C to F) *In vitro*-transcribed RNA encompassing SL1, -2, and -3, with a poly(A) tail of 27 nucleotides in length, was subjected to limited RNase digestion with dilutions of RNases and to subsequent primer extension analysis. A sequencing ladder obtained using the same primer allows the identification of the RNase cleavage sites. Analysis was performed a minimum of three times, and one representative gel is shown. Nucleotide positions are numbered according to their positions in the murine norovirus genome. Note that data are shown for regions containing RNase cleavage sites only.

initial MOI of 4, with samples taken in triplicate for TCID$_{50}$ titration and singularly for Western blot analysis, at 0, 4, 6, 8, 12, and 24 h postinfection (hpi). Multistep growth curve analysis was performed using an MOI of 0.01, with harvest at 0, 6, 12, 24, and 48 hpi. RAW 264.7 cells were plated in 2-cm^2 wells at a density of 2×10^5/well, while BMMs were plated at double this density (4×10^5/well).

Viral sequence analysis. Sequences were aligned using the ClustalW program imbedded in the AlignX subprogram of Vector NTI 11 (Invitrogen). RNA structure predictions were performed using the online mfold and Vienna software, available at http://mfold.bioinfo.rpi.edu/cgi-bin/rna-form1.cgi (48) and http://rna.tbi.univie.ac.at/cgi-bin/RNAfold.cgi, respectively.

Viral competition analysis. Wild-type and SL3 GNRA viruses were mixed at a 1:1 ratio (based on TCID$_{50}$) and used to infect RAW 264.7 cells (1.2×10^6/well in a 9-cm^2 dish) at an overall MOI of 0.01. At 48 h postinfection, the virus was extracted as detailed above, and the resultant mixed population was used to infect an equivalent dish of RAW cells at a low MOI (approximately 0.01). RNAs were extracted for sequencing after an additional passage of the mixed population at a high MOI (>1) in RAW cells. The 3′ end of the MNV genome was sequenced to quantify the relative abundances of both wild-type and SL3 GNRA viruses. The process was repeated for five passages, with virus and RNA being extracted at each step. As additional controls, both wild-type and SL3 GNRA viruses were passed alone on RAW cells for 5 rounds of infection, using an identical passage regimen. These viruses were also equivalently sequenced to confirm the stability of wild-type and SL3 GNRA 3′ sequences.

Virulence studies. Sex-matched STAT1$^{-/-}$ mice (Taconic) were inoculated by oral gavage with 1,000 TCID$_{50}$ of either wild-type (v) or SL3 GNRA (v) virus (group size, 8 males and 8 females per virus). Mock inoculations for the negative control group were performed using an uninfected lysate from RAW 264.7 cells prepared in an identical manner to that for the virus stocks (group size, 6 males and 3 females). Animals were monitored daily for the onset of disease, which is characterized by weight loss, piloerection, anorexia, and eye discharge. The development of serious MNV-induced disease is characterized by serious weight loss, ataxia, moribundity, and eventually death. Where possible, the development of serious disease prompted euthanasia to avoid undue suffering to the animal. A humane end point of 25% weight loss was also set. On days 3 and 5 postinfection, 2 males and 2 females from the two virus groups were euthanized, and the following tissues and samples were removed and placed in Trizol solution (Invitrogen) during postmortem: spleen, mesenteric lymph node, kidney, liver, small intestine, heart, lung, and feces (removed *in situ* from the colon). Equivalent tissues were taken from animals in the mock lysate group at 14 days postinfection, which represented the end of the experiment due to lab restrictions as well as the outcome and severity of infection. RNA was extracted from tissues as detailed in the Trizol manufacturer's instructions.

Quantitative real-time reverse transcription-PCR. RNA was reverse transcribed to cDNA by use of oligonucleotide IC464 (CAAACATCTTTCCCTTG TTC) and AMV reverse transcriptase (Promega) as detailed in the manufacturer's instructions. cDNA was amplified by real-time PCR, using qPCR master mix (Eurogentec) and an ABI 7900 real-time PCR machine. Briefly, cDNA was mixed with 2× buffer and primers IC464 and IC465 (TGGACAACGTGGTGA AGGAT) in the PCR plate, heat denatured to 95°C for 10 min, and subjected to 40 cycles of 94°C for 15 s, 58°C for 30 s, and 72°C for 30 s. Viral genome copy number was calculated by interpolation from a standard curve. This was generated using serial dilutions of standard RNA representing nucleotides 1085 to 1986 of the MNV genomic RNA, generated by *in vitro* transcription. Standard RNA was PAGE purified, phenol chloroform extracted, ethanol precipitated, resuspended in nuclease-free water, and quantified using spectrophotometry.

RESULTS

The MNV genome contains three stem-loop structures at the 3′ end. Our previous bioinformatic analysis identified the presence of a region of significant synonymous codon suppression at the 3′ end of the VP2 coding region, as well as conserved RNA structures within the 3′-untranslated region (3′-UTR) (Fig. 1) (35). In addition, alignment of a number of previously published sequences demonstrated the existence of polymorphism in the length of the polypyrimidine tract [referred to herein as the p(Y) tract] predicted to lie within the terminal loop sequence (data not shown). To further confirm the presence of defined RNA structures within the 3′ end of

the MNV genome, we used biochemical structure probing with conformation-specific RNases, followed by reverse transcription to identify the positions of RNase digestion (Fig. 1B–F). This confirmed the presence of the three bioinformatically predicted stem-loop structures, depicted as SL1 to SL3 in Fig. 1B. Only a limited number of double-strand-specific RNase V1 digestion sites were observed in the 5′-proximal stem-loop (SL1), suggesting that these regions are not accessible to digestion or do not adopt the correct helical conformation required for efficient cleavage (24). In addition, some regions of SL1 predicted to be double stranded were sensitive to cleavage with single-strand-specific RNases (e.g., G7286), possibly reflecting the inherent instability or flexibility of the RNA surrounding that particular sequence. While it is feasible that the predicted structure for SL1 may be incorrect, the high degree of conservation and the presence of (limited) covariation in this stem (Fig. 1B) argue for alternative interpretations. In addition, the predicted thermodynamic stability of SL1 is very favorable, presenting further supporting evidence for its existence (data not shown). The structures of SL2 and -3 were better defined using biochemical structure probing, with clear regions showing sensitivity to single- and double-strand-specific RNases (Fig. 1B–F).

Functional requirements of RNA structures in the MNV 3′ UTR. To determine the functions of the RNA structures present in the 3′ UTR and to identify sequences and/or structures required for norovirus replication and virulence, a panel of deletion and point mutations in the MNV1 3′ end were generated (Fig. 2). The SL3 ssm (secondary structure mutant) mutation has been described previously and referred to as m54 (35). Infectious clones containing the various mutations in the MNV 3′ end were transfected into cells previously infected with a helper virus expressing T7 RNA polymerase as described previously (7), and the ability to recover infectious virus was determined (Table 1). Complete deletion of the GA-rich tract of SL2 or deletion of SL3 or both SL2 and -3 rendered the clone noninfectious (Table 1), confirming that the integrity of the entire 3′ UTR is critical for function. In addition, we failed to recover any viable virus after repeated "blind" passage of the samples obtained from the virus recovery transfections, confirming the debilitating effects of the deletion mutations.

To exclude the possibility that the debilitating effect of deletion of the GA-rich tract of SL2 on MNV replication was simply related to alterations in the spatial relationship of SL1 and SL3, which would be 10 nucleotides closer together in the ΔSL2 virus than in the wild-type virus, we also examined the effect of sequence alterations to SL2 on MNV replication (SL2 ssm) (Fig. 2). The SL2 ssm virus was designed to replace the GA-rich sequence with an unrelated sequence of different composition which would also disrupt the stability of SL2 without affecting the structure of SL1 and SL3. As with the ΔSL2 GA virus, the mutations introduced into the SL2 ssm mutant were debilitating for MNV replication, and no infectious virus could be recovered, despite repeated blind passage of the virus recovery transfections.

We have previously demonstrated that alterations to the structure of SL3 are debilitating to MNV replication (35), as the mutant referred to herein as SL3 ssm (Fig. 2) (called m54 in reference 35) failed to produce detectable levels of infec-
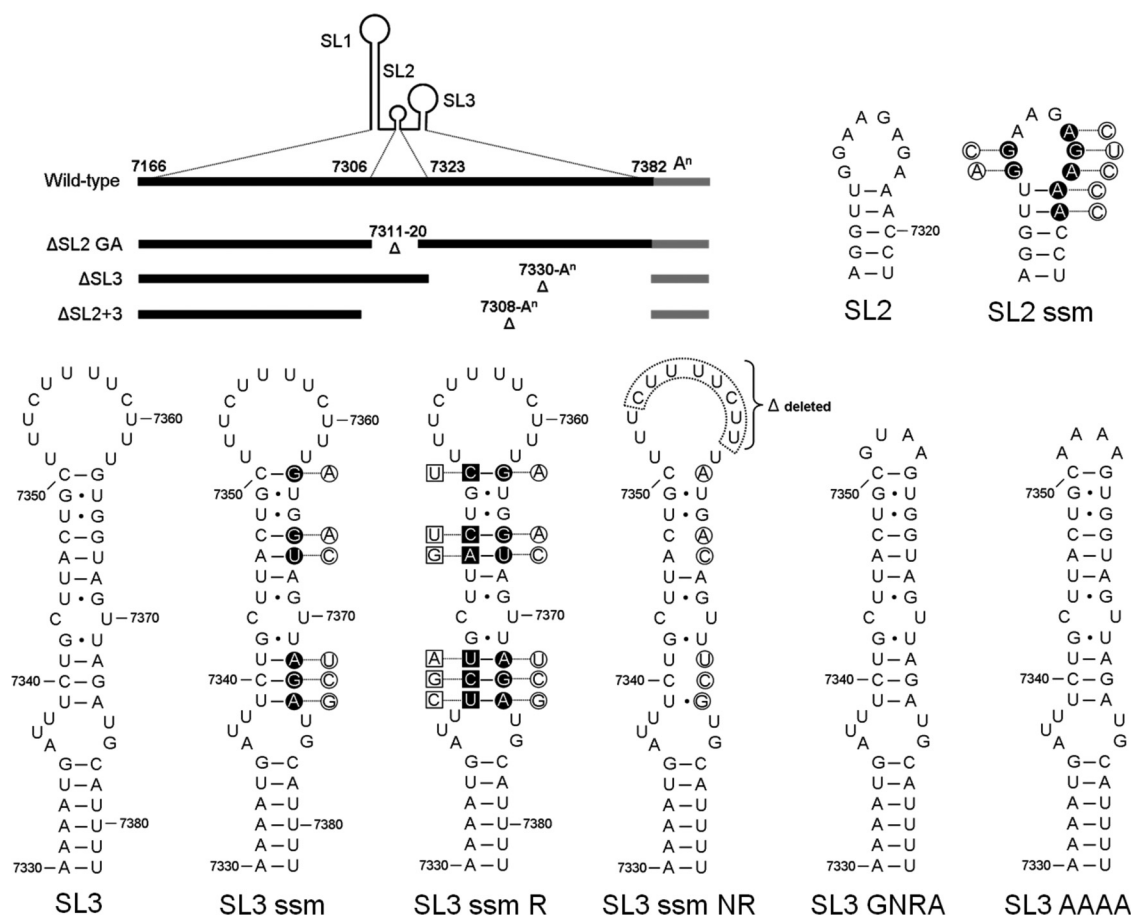
FIG. 2. Murine norovirus 3′-end mutants. Schematic representation of the MNV 3′ end, highlighting the various deletion and point mutants under study. The diagram at the top left highlights the nucleotide positions of the various stem-loops, SL1 to SL3, and the GA-rich sequence in SL2 deleted in the corresponding mutants. The positions of the nucleotide alterations in SL2 ssm, SL3 ssm, and SL3 ssm R are highlighted with filled circles or squares, with the corresponding changes introduced shown offset in the open circles or squares. The predicted secondary structures of SL3 in the SL3 ssm NR mutant, with the deleted sequence boxed, in SL3 GNRA, and in SL3 AAAA are also shown. Note that for the purposes of this figure, the base pairing predicted to occur between the poly(A) tail and the MNV 3′ UTR has been omitted. In addition, the schematics for SL2 ssm, SL3 ssm, SL3 ssm R, and SL3 ssm NR are for illustrative purposes only, since the predicted secondary structure is significantly modified by the introduced mutations.

tious virus after the initial reverse genetics recovery transfection (Table 1). To determine whether the sequence of or base pairing in the stem region of SL3 was required for replication, a number of restorative mutations were introduced into SL3 ssm to restabilize the structure (SL3 ssm R) (Fig. 2). Restoration of the SL3 base pairing did not, however, result in the recovery of infectious virus, indicating that at least some of the sequence within the stem also plays an important role. Interestingly, however, repeated blind passage of the parental SL3 ssm mutant resulted in the generation of a virus which had regained the ability to replicate. Sequence analysis of the isolated virus, referred to as SL3 ssm NR (for natural revertant), indicated that the initial mutations in the stem were still present but that a substantial 8-nucleotide deletion of the p(Y) tract had occurred (Fig. 2).

The 3′ p(Y) tract binds the cellular polypyrimidine tract binding protein and poly(rC) binding protein. Two well-characterized host cell factors with the capacity to bind pyrimidine-rich sequences are poly(rC) binding proteins (isoforms 1 and 2 [PCBP1/2]) (25) and polypyrimidine tract binding protein

TABLE 1. Effects of mutations in MNV 3′ end on virus recovery, using reverse genetics

Mutation	Description	Recovery[a]
ΔSL2 GA	Deletion of stem-loop 2 positions 7311 to 7320	No
ΔSL3	Deletion of stem-loop 3 position 7330 to poly(A)	No
ΔSL2 + 3	Deletion of stem-loops 2 and 3 from position 7308 to poly(A)	No
SL2 ssm	Mutation disrupting secondary structure in SL2 stem and loop	No
SL3 ssm	Mutation disrupting secondary structure in SL2 stem[b]	No
SL3 ssm R	Secondary structure reversion mutant of SL3 ssm	No
SL3 GNRA	Substitution of polypyrimidine tract loop in SL3 with GNRA tetraloop	Yes
SL3 AAAA	Substitution of polypyrimidine tract loop in SL3 with AAAA tetraloop	Yes

[a] Virus recovery is defined as the ability to generate virus capable of generating clear cytopathic effect in RAW 264.7 cells by 5 days postinfection. The limit of detection of this assay was ~50 $TCID_{50}$/ml. Each recovery was repeated a minimum of three times and was scored as negative if no detectable virus was observed. The yields of wild-type, SL3 GNRA, and SL3 AAAA cDNA clones were typically >10^4 $TCID_{50}$ per 35-mm dish.

[b] A natural revertant of this virus (SL3 ssm NR) was generated following multiple blind passages of this virus in permissive cells (as described in the main text).
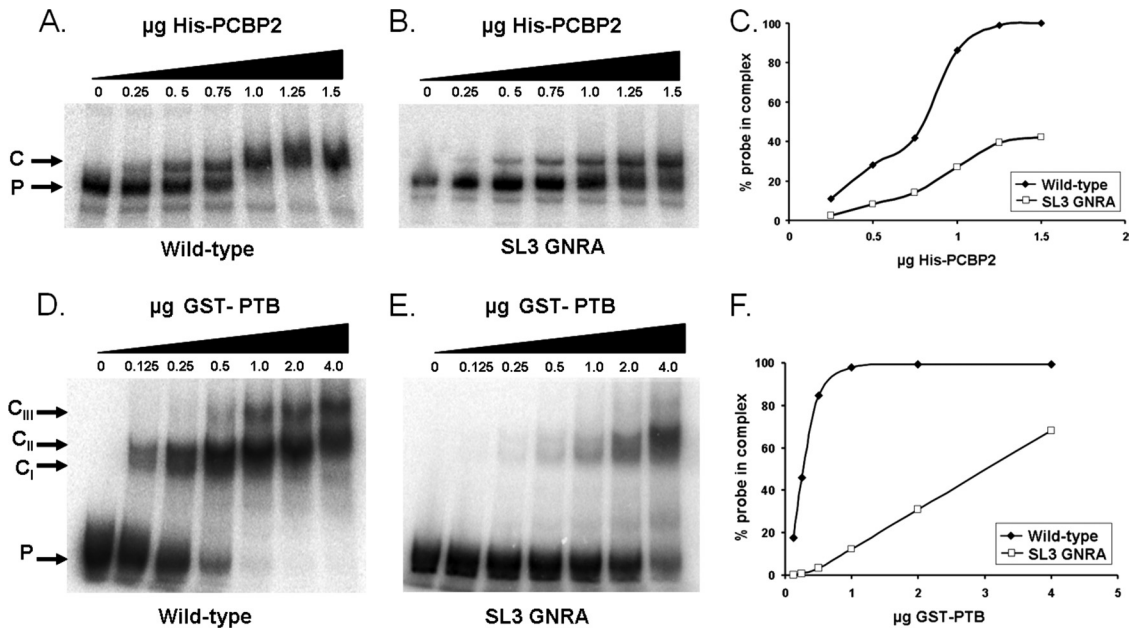
FIG. 3. PCBP2 and PTB binding to the murine norovirus 3′ end. EMSAs demonstrated the ability of recombinant PCBP2 and PTB to interact with the wild-type MNV 3′ end (A and D, respectively) or the SL3 GNRA 3′ end (B and E, respectively). Quantification of the corresponding EMSA products is expressed as the percentage of probe in any complex with either recombinant PCBP2 (C) or PTB (F). The positions of the free probe (P) and various RNA-protein complexes (C, C_I, C_{II}, and C_{III}) are also highlighted.

(PTB) (33). These proteins have previously been identified as components of a ribonucleoprotein complex (RNP) which can form on the 5′ and 3′ ends of the Norwalk virus genome (15, 16). We therefore examined the ability of recombinant forms of PCBP and PTB to bind to the 3′ UTR of the MNV genome by using EMSA (Fig. 3A and D). Our data indicate that both PCBP1 (data not shown) and PCBP2 (Fig. 3A) can interact with the 3′ end of the MNV genome to form a stable RNP complex. Recombinant PTB was also able to form a stable RNP complex with the 3′ end of the MNV genome (Fig. 3D), and as in the case of PCBP, the specificity of the interaction was confirmed by both the inability of heterologous competitor RNA to compete for RNP complex formation and, conversely, the ability of unlabeled homologous RNA to compete (data not shown). Given the previously reported propensity of one of these host cell factors to interact with single-stranded pyrimidine-rich regions (25), we examined the role of the variable p(Y) tract in PCBP and PTB binding by EMSA, using a 3′ end derived from SL3 in which the p(Y) tract was replaced by a GNRA tetraloop (26) (shown as SL3 GNRA in Fig. 2). EMSA data demonstrated a reduced ability for RNP complex formation on the SL3 GNRA probe compared to a wild-type probe (Fig. 3B, C, E, and F), indicating that the p(Y) tract is important for the binding of PCBP and PTB. The binding site for PTB was also confirmed using biochemical RNase footprinting analysis, which demonstrated that the p(Y) tract was the major PTB and PCBP binding site (Fig. 4). Binding of PTB and PCBP2 to the MNV 3′ end did not result in any major effect on the folding of SL1, SL2, or SL3, as is evident from RNase sensitivity mapping (data not shown).

The 3′ p(Y) tract is not required for MNV replication in tissue culture. The isolation of naturally generated replication-
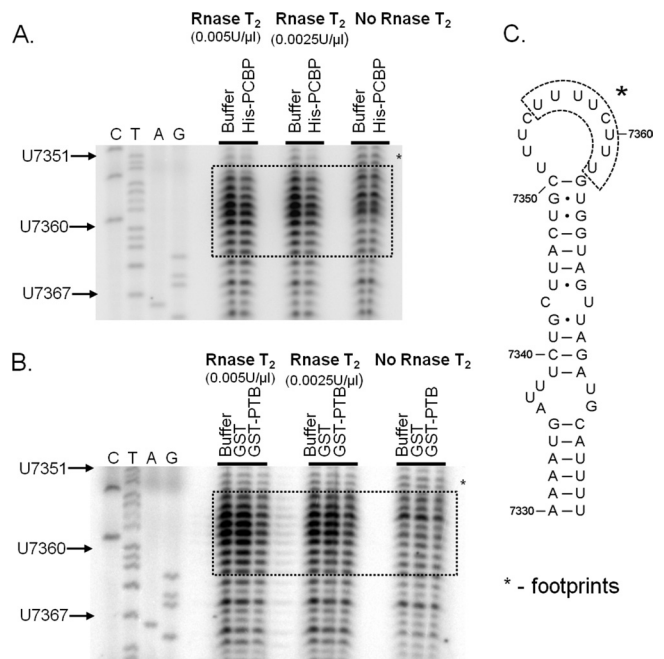

FIG. 4. Biochemical footprinting confirmation of PTB binding site. Polyacrylamide gel analysis was performed on primer extension products obtained from transcripts digested with the single-strand-specific RNase T2 in the presence of PCBP2 (A) or GST, GST-PTB, or buffer alone (B). A sequencing ladder was run alongside, obtained using the same primer, to highlight the sequence protected by PCBP2 and PTB binding (boxed). (C) Schematic representation of SL3 highlighting the PCBP2 and PTB binding site identified by footprinting analysis.
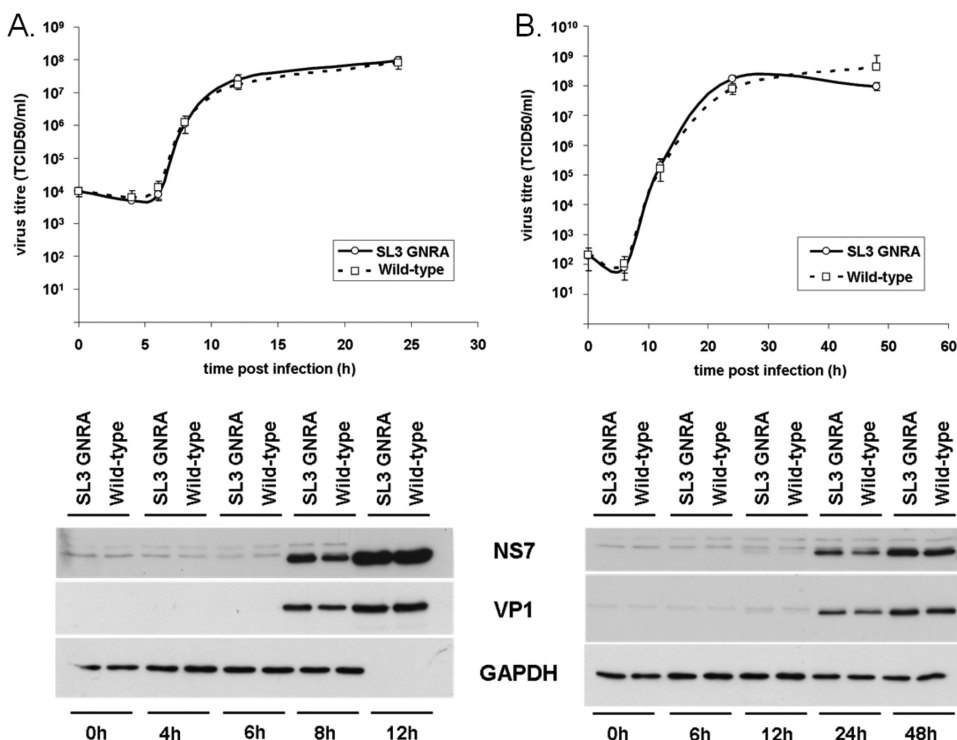
FIG. 5. Viral growth kinetics of wild-type and SL3 GNRA murine noroviruses in tissue culture. Single-cycle (A) and multicycle (B) growth kinetics of wild-type virus and the virus lacking the 3′ p(Y) tract (SL3 GNRA) were determined with the murine macrophage cell line RAW 264.7. Cells were infected at multiplicities of infection of 4 and 0.01 (A and B, respectively), and samples were taken at various time points postinfection. The yield of infectious virus was determined by $TCID_{50}$ titration in RAW264.7 cells and expressed as $TCID_{50}$/ml. Infections were performed in triplicate, and the averages were plotted along with standard deviations. Viral protein synthesis was also examined by preparing protein extracts and subsequently analyzing them by Western blotting of 10 μg of protein for the viral polymerase (NS7), viral capsid (VP1), or an endogenous host cell protein (GAPDH). Note that the absence of GAPDH at 12 h postinfection during the single-cycle growth curve analysis was the likely result of the effect of virus infection on host cell protein synthesis.

competent MNV carrying a deletion within the p(Y) tract suggests that this region may not be required for virus replication in tissue culture. However, this deletion occurred in a mutant containing several destabilizing mutations in the SL3 stem sequence (SL3 ssm in Fig. 2). To specifically analyze the functional requirements for the p(Y) tract, we generated two cDNA clones bearing mutations in the p(Y) tract of SL3, namely, SL3 GNRA, containing a complete replacement of the p(Y) tract with a GNRA stem-loop-stabilizing sequence (GUAA in reference 26), and the SL3 AAAA mutant, containing a tetra-A loop in place of the p(Y) tract (Fig. 2). Reverse genetics recovery of these viruses indicated that they were both replication competent, producing similar levels of virus to those for the wild-type infectious clone (Table 1). To examine any differences in growth kinetics and protein production rates, we performed single-cycle and multicycle growth curve analysis of SL3 GNRA and compared it to wild-type virus (Fig. 5A and B, respectively). No significant differences were apparent in the rates at which infectious virus was produced from RAW 264.7 murine macrophage cells infected with SL3 GNRA or wild-type virus during both single-cycle and multicycle growth (Fig. 5). Analysis of protein production by Western blot analysis for the viral polymerase NS7 and the major capsid protein VP1 showed a small but reproducible increase in NS7 production in cells infected with SL3 GNRA compared to that in cells infected with wild-type virus (Fig. 5A

and B). A reproducible loss of the cellular glyceraldehyde-3-phosphate dehydrogenase (GAPDH) protein was also observed during the later stages of viral single-cycle infection (Fig. 5A).

Deletion of the 3′ p(Y) tract results in a fitness cost to MNV replication. The observation that all sequenced MNV isolates identified to date possess a p(Y) tract in the 3′ UTR, although the sequence and length can vary (data not shown), suggests that the presence of the 3′ p(Y) tract confers some fitness benefit to MNV. However, our reverse genetics and growth curve data indicated that it was nonessential for growth in RAW 264.7 murine macrophage cells. The stability of the SL3 GNRA mutant was therefore examined over repeated passage in tissue culture at a low multiplicity of infection. Sequence analysis of the virus population indicated that the GNRA mutation was still present after repeated passage in tissue culture (data not shown). To further determine if the deletion of the p(Y) tract resulted in a fitness cost that was not apparent in the absence of additional external selective pressures, we examined the ability of the SL3 GNRA mutant virus to replicate in the presence of wild-type virus. Wild-type and SL3 GNRA viruses were mixed at a ratio of 1:1 and subsequently repeatedly passaged in murine RAW 264.7 macrophage cells. The sequence of the 3′ UTR was subsequently analyzed during the various passages by sequencing of the viral population (Fig. 6). Although the sequence obtained after passage 1 showed that
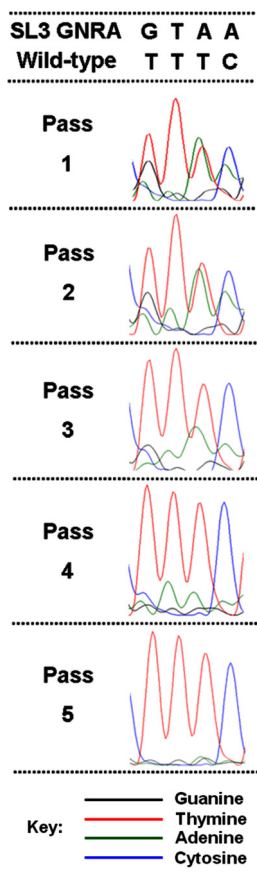
FIG. 6. Competition analysis of wild-type and SL3 GNRA murine noroviruses. Sequencing chromatograms were obtained for the virus population obtained after 1 to 5 passages of a 1:1 mix of wild-type and SL3 GNRA viruses in RAW 264.7 cells. Cells were infected at an approximate multiplicity of infection of 0.01 for 48 h before dilution and passage onto an additional monolayer. For virus sequence analysis, the virus population isolated at each passage was used to infect a fresh monolayer at a high multiplicity of infection (>3) for ~16 h before viral RNA was extracted from the cells and sequenced by reverse transcription-PCR.
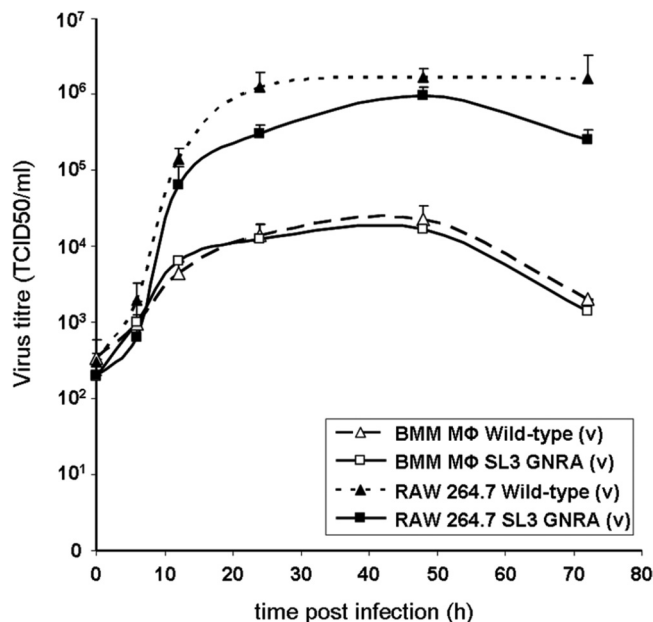

FIG. 7. Viral growth kinetics of virulent wild-type and SL3 GNRA viruses in primary bone-derived murine macrophage cells. Sequence-verified stocks of wild-type or SL3 GNRA murine norovirus in the CW1.P1 backbone (see the text for more details) were used to infected either RAW 264.7 cells or primary bone-derived macrophage cells at a multiplicity of infection of 0.01 (based on viral titration in RAW 264.7 cells). Infections were performed in triplicate, and samples were taken at various times postinfection prior to $TCID_{50}$ titration in RAW 264.7 cells. The average titers were plotted as $TCID_{50}$/ml, with the standard deviations also shown.

both wild-type and SL3 GNRA viruses were present at comparative levels (as evident by the heterogeneity at the first, third, and fourth nucleotide positions), by passage 5 the sequence of the wild-type virus predominated (Fig. 6), indicating that the presence of the 3′ p(Y) tract conferred a competitive advantage to this virus during MNV replication in tissue culture. Equivalent observations were recorded in two independent repeats of this 1:1 experiment, and even at a 1:10 ratio (wild type to SL3 GNRA) (data not shown).

The 3′ p(Y) tract contributes to MNV virulence. To determine if the 3′ p(Y) tract plays a role in viral virulence *in vivo*, we first introduced the SL3 GNRA 3′ end into an MNV1 cDNA clone containing two mutations (G2151A and A5941G). This sequence more faithfully represents the consensus sequence isolated from infected $STAT1^{-/-}$ mice (referred to as CW1.P1 in references 1 and 19), and we have previously demonstrated that the A5941G mutation, which results in a change of glutamate 296 to lysine in the major capsid protein VP1, is sufficient to restore virulence to the

tissue culture-adapted attenuated strain of MNV (1). As observed in the attenuated virus background, the derivatives of the wild-type and SL3 GNRA mutant viruses in the virulent background [wild type (v) and SL3 GNRA (v)] replicated to similar levels in both RAW 264.7 cells and primary bone marrow-derived macrophages (Fig. 7). The role of the 3′ p(Y) tract in viral virulence was then examined by oral inoculation of $STAT1^{-/-}$ mice with the wild-type (v) and SL3 GNRA (v) viruses (Fig. 8). Control inoculated mice continued to gain weight throughout the duration of the study, whereas mice inoculated with wild-type (v) MNV showed statistically significant weight loss at 4 days postinoculation ($P < 0.001$ by analysis of variance [ANOVA]) (Fig. 8). In contrast, weight loss in the SL3 GNRA (v)-inoculated mice was more varied, with some mice displaying similar weight losses to those of the wild-type (v) group at 4 days postinfection while others continued to gain weight in a comparable manner to the mock-infected group. Significant weight loss in the SL3 GNRA (v)-infected mice (compared to the control group) was not observed until 5 days postinfection.

Comparisons of weight losses between SL3 GNRA (v)- and wild type (v)-inoculated mice showed significant variation at days 4, 5, and 6 postinfection ($P < 0.05$, $P < 0.001$, and $P < 0.001$, respectively, by ANOVA) (Fig. 8A), indicating a marked deviation from normal disease progression. The symptomatic onset of disease and associated mortality also reflected this variation between the wild-type and mutant viruses. On day 5 postinfection, 5 of 12 mice infected with wild-type (v) virus had
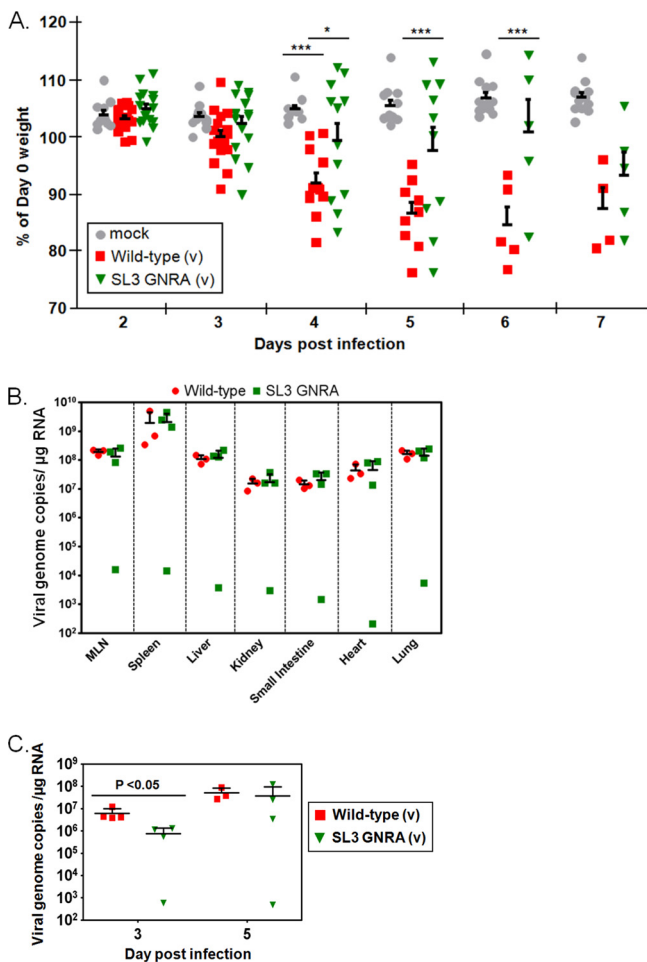
FIG. 8. Virulence analysis of wild-type and SL3 GNRA murine noroviruses in STAT1$^{-/-}$ mice. (A) Age- and sex-matched groups of STAT1$^{-/-}$ mice were orally inoculated with 1,000 TCID$_{50}$ of sequence-verified, partially purified wild-type or SL3 GNRA murine norovirus recovered in the virulent backbone (see the text for details), and their weight was monitored daily. Control mice were inoculated with a lysate from cells prepared in a similar manner to that for the virus stocks (see Materials and Methods for further details). ∗∗∗, $P <$ 0.001; ∗, $P < 0.05$ by two-way ANOVA with Bonferroni posttests. (B) qPCR with tissues; (C) qPCR with feces. The numbers of viral genome copies were determined by quantitative real-time reverse transcription-PCR. RNAs were extracted from numerous tissues at 5 days postinfection and from feces at 3 and 5 days postinfection, and the numbers of genome copies per μg of total RNA were determined as described in Materials and Methods. The means are shown, with standard errors highlighted. The significant difference recorded at day 3 postinfection was observed using a standard t test.

succumbed to infection or had passed the established humane end points and been euthanized, with an additional animal being moribund. All remaining animals in this group showed the established clinical signs and symptoms of infection, i.e., weight loss, piloerection, discharge from the eyes, associated depressed motility, and anorexia. In contrast, the SL3 GNRA (v) group showed noticeable variation in both the onset of disease symptoms and the establishment of clinical signs. By day 5, two animals had succumbed to infection, one was moribund, and three exhibited weight loss and symptoms of disease. However, six showed no clinical signs or symptoms of

infection (with all weighing more than their individual day 0 weights) (Fig. 8a), which is a significantly greater proportion than that found in the wild-type-infected control group ($P = $ 0.014 by two-tailed Fisher's exact test). Note that all animals infected with SL3 GNRA (v) eventually established disease symptoms and clinical signs of infection. Postmortem analysis of animals euthanized for tissue sampling on days 3 and 5 postinfection also highlighted differences between SL3 GNRA (v)- and wild-type (v)-infected mice, which typically correlated with the differential weight loss evident in the two groups. Animals with significant weight loss showed more serious pathological signs of infection, such as liver and spleen necrosis, gastric bloating, and significant dehydration. However, those animals exhibiting weight gain or reduced weight loss [found more frequently in SL3 GNRA (v)-infected mice] (Fig. 8A) were often normal upon postmortem. This correlated with the distribution of viral RNA within various tissues of the host, which was examined using quantitative real-time PCR (Fig. 8B). While all mice infected with wild-type (v) virus contained high levels of viral RNA in their tissues on days 3 and 5 postinfection, only 75% of SL3 GNRA (v)-infected mice had equivalent levels of viral RNA (Fig. 8B; data not shown for day 3, but the trend was comparable). Note that animals were arbitrarily selected for tissue sampling based on ear tag number, not the presence of disease. Significantly, the levels of excreted viral RNA obtained from feces taken from the colon during postmortem were found to be reduced in the SL3 GNRA (v)-inoculated mice at 3 days postinfection compared to those inoculated with the wild-type (v) virus (Fig. 8C).

DISCUSSION

The study of RNA-protein interactions required for calicivirus translation and/or replication has, to date, largely been limited to *in vitro* analysis. The well-characterized cellular nucleic acid binding proteins PTB, PCBP, La autoantigen, and hnRNP L have all previously been reported to interact with the 5′ end of the Norwalk virus genome (15), whereas La and PTB, along with poly(A) binding protein, have also been shown to interact with the 3′ UTR (16). One or more of these host cell factors or an as yet unidentified factor may be involved in protein-mediated circularization of the Norwalk virus genome (32). As is well established for other positive-strand RNA viruses, host cell factors may similarly interact with RNA structures and/or sequences within the norovirus genome and play roles in the viral life cycle. To date, however, no functional interaction between a host protein and the norovirus genome has been demonstrated, although it has been shown that the interaction of PTB with the genome of feline calicivirus (FCV), another member of the *Caliciviridae* family, plays some role in the virus life cycle (18).

In the current study, we aimed to identify and characterize RNA structures/sequences at the 3′ end of the viral genome that are required for norovirus replication, using MNV as a model system. The use of MNV as a model system also subsequently allowed us to extend these studies to examine, for the first time, the role of RNA structures in norovirus virulence. Biochemical analysis of the structure of the 3′ end of the MNV genome revealed that in agreement with our previously reported bioinformatic analysis (35), the MNV genome con-

tains three putative stem-loops within the 3′ end of the viral genome, one within the VP2 coding region and two within the UTR, although the stop codon of VP2 also contributes two nucleotides to SL2 (Fig. 1). SL1 was largely insensitive to RNase digestion, and only a limited number of cleavage sites were identified (Fig. 1). Although our current study did not confirm a functional role for SL1, bioinformatic analysis demonstrates that as with SL2 and SL3, SL1 shows restricted genetic variability compared to neighboring coding sequences, with covariation to maintain pairing for substitutions occurring in predicted base-paired regions of the stem (Fig. 1B). The presence of a functional *cis*-acting RNA structure within the VP2 coding region has already been reported for another member of the *Caliciviridae*, namely, FCV (36). Previous analysis demonstrated that although the FCV VP2 protein is required for infectious virion production, the underlying VP2 coding sequence contains an element (or elements) required in *cis* for genome replication to occur (36). The boundaries of this replication element indeed map exactly to the predicted large stem-loop structure in this region of VP2 (35), and it is similar in size and position to SL1 in MNV. Although MNV, FCV, and GII/4 human noroviruses contain potential RNA structures within the VP2 coding region, secondary structure elements do not appear to be universally present in all members of the *Caliciviridae*; previous bioinformatic analysis provided no evidence for conserved RNA secondary structures in the homologous region for members of the *Lagovirus* genus (35). Furthermore, unlike the case with FCV, complete removal of the VP2 coding sequence from the genome of rabbit hemorrhagic disease virus (RHDV) had little effect on virus replication in tissue culture (23). Recent work has also highlighted that sequences within the 3′ end of the Norwalk virus genome contain an RNA element or elements which stimulate the *in vitro* nucleotidylation of recombinant VPg in the presence of magnesium chloride (2). This may suggest that similar to previous reports for poliovirus (11, 29), the norovirus genome may possess sequences which may function as a template for the transfer of nucleotide to VPg to allow genome replication. Clearly, additional data are required to identify the specific sequences involved and to confirm their role in VPg-dependent genome replication.

The identification of a natural revertant of the SL3 ssm mutant, with a disrupted terminal stem-loop (SL3) in which the p(Y) tract was deleted, indicates that this sequence is not required for MNV replication *in vitro*. SL3 ssm mutations in SL3 (in the context of the 3′ end of the viral genome) create an alternative possible RNA structure containing a stable stem in which the GA-rich sequence of SL2 interacts with the p(Y) tract of SL3 (data not shown). This base paring in the SL3 ssm mutant therefore completely disrupts SL2 and SL3. Prediction of the structure adopted by the SL3 ssm NR 3′ end indicates that the observed deletion in the p(Y) tract allows the formation of SL2 and the bottom stem of SL3 when the SL3 ssm mutations are also present (data not shown). These data suggest that the stability and correct formation of SL2 and the bottom stem of SL3 are critical for MNV replication. Our previous observation that replacement of the terminal U nucleotide with a C resulted in a complete loss of MNV viability (7) also indicates that the terminal stem is important for replication. Combining our current and previous data, we can conclude that SL2 and the bottom stem of SL3 are essential for MNV viability. Further studies will be aimed at identification of the host cell or viral factors which interact with these regions and determination of the functional defect in viruses bearing mutations in these regions.

We demonstrated a sequence-specific interaction of PCBP1/2 and PTB with the variable p(Y) tract in the 3′ end of the MNV genome, although this interaction appears to be nonessential for virus replication *in vitro*. A reproducible increase in the levels of proteins produced from a virus lacking the p(Y) tract was observed, although this clearly had no detectable effect on virus titer (Fig. 5). This might suggest that the 3′ p(Y) tract plays some role in controlling the balance between viral genome translation and replication or that the binding of PCBP1/2 and/or PTB to this region has a repressive effect on virus translation. In addition to the interactions of PCBP1/2 and PTB with the 3′ end reported here, we have recently shown that PCBP1/2 and PTB also have the ability to interact with the 5′ ends of the MNV genomic and subgenomic RNAs (I. Karakasiliotis, L. M. W. Chung, and I. Goodfellow, unpublished data). It is therefore possible that PCBP1/2 or PTB interacts simultaneously with the 5′ and 3′ ends of the MNV genome to result in genome circularization, as is predicted to occur in Norwalk virus (32), but further studies are required to examine this in more detail. Despite the ability of the SL3 GNRA virus to replicate, our competition analysis indicated that the deletion of the p(Y) tract resulted in a fitness cost (Fig. 6), which may explain why this region, although variable in size, is present in all isolates of MNV identified to date. Although PCBP1/2 and PTB binding was significantly reduced by the replacement of the p(Y) tract with a GNRA tetraloop, it was not abolished, as some residual (but specific) binding activity remained (Fig. 3C and F). Residual binding may have been sufficient to allow replication to occur in rapidly dividing cells in cell culture, where the levels of factors such as PCBP1/2 and PTB are likely to be substantially higher than those in differentiated tissues *in vivo*. Other host cell factors may also be overexpressed in immortalized cells and effectively complement the lack of PCBP1/2 or PTB binding. Similarly, the residual PCBP1/2 and PTB binding may also explain the reduced virulence of the SL3 GNRA virus in the STAT1$^{-/-}$ mouse model. Given the additional selective pressures on virus replication *in vivo*, one possible explanation for the subsequent disease progression in mice inoculated with the SL3 GNRA virus was that viruses regained the p(Y) tract. However, sequence analysis of viruses isolated from the various tissues indicated that reversion or restoration of the p(Y) tract had not occurred either in those animals that lost weight equivalently to wild-type-infected mice or in those that did not (data not shown). The evidence for a functional role of the p(Y) tract for *in vivo* replication may indeed contribute to the ability of MNV to establish persistent infections in immunocompetent hosts (17, 40). Indeed, a more evident role for the p(Y) tract may be revealed in future challenge experiments using immunocompetent mice in place of the STAT1$^{-/-}$ mice used in the current study. To date, however, a reverse genetics system for an MNV isolate which results in a persistent infection has yet to be established.

The presence of a p(Y) tract within the 3′ UTR of MNV is not unique to MNV, as many positive-strand RNA viruses

contain such elements. The 3′ UTR of hepatitis C virus (HCV) also contains a p(Y) tract, of ~200 nucleotides in length (21, 39, 45), which interacts with hnRNPC and PTB (10). In contrast to our current studies with MNV, however, the HCV p(Y) tract is essential for HCV replication in tissue culture, requiring a minimum length of 26 U residues for replication (9). The 3′ p(Y) tract of HCV has also been shown to be important for viral virulence, as deletions inhibit virus recovery after hepatic inoculation of *in vitro*-transcribed viral RNA (46). The function of the HCV 3′ p(Y) tract is as yet unknown, but data indicate that it may play a stimulatory role in viral internal ribosome entry site (IRES)-mediated translation (43).

The attenuation of positive-strand RNA viruses through the modification of RNA structures present in the 5′ or 3′ end of the viral genome has been well documented for many different viruses. For example, attenuation of West Nile virus can be achieved through the modification of sequences within the 3′-terminal stem-loops (47). Some deletions in the 3′ UTR of foot-and-mouth disease virus (FMDV) also affect virulence but not tissue culture growth, and in this case, they were found to elicit a protective immune response in swine (30). One of the best-characterized examples of where the interaction of a host cell factor with viral RNA structures plays a role in pathogenesis is in the attenuation of poliovirus, where mutations in the 5′ UTR of vaccine strains affect the binding of PTB (14) and other translation initiation factors (28). *In vivo* studies also confirmed the importance of the interaction of PTB with these sequences for poliovirus neurovirulence (12). Here we describe how reverse genetics can also be used as a potential method to attenuate murine norovirus via the modification of noncoding sequences. Previous studies have clearly indicated that live virus vaccination against noroviruses can be effective (4), and hence, once a full infectious tissue culture system is established, this and similar approaches which generate live attenuated noroviruses may provide a mechanism for vaccinating against human norovirus infection. Clearly, such studies will only be feasible once the "missing link" which allows human norovirus replication to occur in tissue culture has been identified; recent studies suggest that this is at the level of virus entry and uncoating (13). Until that point, studies such as that described here will continue to add to our growing understanding of norovirus-host cell interactions, potentially leading to novel approaches for the control of this economically important pathogen.

REFERENCES

1. **Bailey, D., L. B. Thackray, and I. G. Goodfellow.** 2008. A single amino acid substitution in the murine norovirus capsid protein is sufficient for attenuation in vivo. J. Virol. **82:**7725–7728.
2. **Belliot, G., S. V. Sosnovtsev, K. O. Chang, P. McPhie, and K. Y. Green.** 2008. Nucleotidylylation of the VPg protein of a human norovirus by its proteinase-polymerase precursor protein. Virology **374:**33–49.
3. **Buchholz, U. J., S. Finke, and K.-K. Conzelmann.** 1999. Generation of bovine respiratory syncytial virus (BRSV) from cDNA: BRSV NS2 is not essential for virus replication in tissue culture, and the human RSV leader region acts as a functional BRSV genome promoter. J. Virol. **73:**251–259.
4. **Chachu, K. A., A. D. LoBue, D. W. Strong, R. S. Baric, and H. W. Virgin.** 2008. Immune mechanisms responsible for vaccination against and clearance of mucosal and lymphatic norovirus infection. PLoS Pathog. **4:**e1000236.
5. **Chang, K.-O., S. V. Sosnovtsev, G. Belliot, A. D. King, and K. Y. Green.** 2006. Stable expression of a Norwalk virus RNA replicon in a human hepatoma cell line. Virology **353:**463–473.
6. **Chang, K. O., D. W. George, J. B. Patton, K. Y. Green, and S. V. Sosnovtsev.** 2008. Leader of the capsid protein in feline calicivirus promotes replication of Norwalk virus in cell culture. J. Virol. **82:**9306–9317.
7. **Chaudhry, Y., M. A. Skinner, and I. G. Goodfellow.** 2007. Recovery of genetically defined murine norovirus in tissue culture by using a fowlpox virus expressing T7 RNA polymerase. J. Gen. Virol. **88:**2091–2100.
8. **Chen, S. Y., C. N. Tsai, M. W. Lai, C. Y. Chen, K. L. Lin, T. Y. Lin, and C. H. Chiu.** 2009. Norovirus infection as a cause of diarrhea-associated benign infantile seizures. Clin. Infect. Dis. **48:**849–855.
9. **Friebe, P., and R. Bartenschlager.** 2002. Genetic analysis of sequences in the 3′ nontranslated region of hepatitis C virus that are important for RNA replication. J. Virol. **76:**5326–5338.
10. **Gontarek, R. R., L. L. Gutshall, K. M. Herold, J. Tsai, G. M. Sathe, J. Mao, C. Prescott, and A. M. Del Vecchio.** 1999. hnRNP C and polypyrimidine tract-binding protein specifically interact with the pyrimidine-rich region within the 3′NTR of the HCV RNA genome. Nucleic Acids Res. **27:**1457–1463.
11. **Goodfellow, I. G., Y. Chaudhry, A. Richardson, J. M. Meredith, J. W. Almond, W. S. Barclay, and D. J. Evans.** 2000. Identification of a *cis*-acting replication element (CRE) within the poliovirus coding region. J. Virol. **74:**4590–4600.
12. **Guest, S., E. Pilipenko, K. Sharma, K. Chumakov, and R. P. Roos.** 2004. Molecular mechanisms of attenuation of the Sabin strain of poliovirus type 3. J. Virol. **78:**11097–11107.
13. **Guix, S., M. Asanaka, K. Katayama, S. E. Crawford, F. H. Neill, R. L. Atmar, and M. K. Estes.** 2007. Norwalk virus RNA is infectious in mammalian cells. J. Virol. **81:**12238–12248.
14. **Gutierrez, A. L., M. DenovaOcampo, V. R. Racaniello, and R. M. delAngel.** 1997. Attenuating mutations in the poliovirus 5′ untranslated region alter its interaction with polypyrimidine tract-binding protein. J. Virol. **71:**3826–3833.
15. **Gutierrez-Escolano, A. L., Z. U. Brito, R. M. del Angel, and X. Jiang.** 2000. Interaction of cellular proteins with the 5′ end of Norwalk virus genomic RNA. J. Virol. **74:**8558–8562.
16. **Gutierrez-Escolano, A. L., M. Vazquez-Ochoa, J. Escobar-Herrera, and J. Hernandez-Acosta.** 2003. La, PTB, and PAB proteins bind to the 3(′) untranslated region of Norwalk virus genomic RNA. Biochem. Biophys. Res. Commun. **311:**759–766.
17. **Hsu, C. C., L. K. Riley, and R. S. Livingston.** 2007. Molecular characterization of three novel murine noroviruses. Virus Genes **34:**147–155.
18. **Karakasiliotis, I., Y. Chaudhry, L. O. Roberts, and I. G. Goodfellow.** 2006. Feline calicivirus replication: requirement for polypyrimidine tract-binding protein is temperature dependent. J. Gen. Virol. **87:**3339–3347.
19. **Karst, S. M., C. E. Wobus, M. Lay, J. Davidson, and H. W. T. Virgin.** 2003. STAT1-dependent innate immunity to a Norwalk-like virus. Science **299:**1575–1578.
20. **Khan, R. R., A. D. Lawson, L. L. Minnich, K. Martin, A. Nasir, M. K. Emmett, C. A. Welch, and J. N. Udall, Jr.** 2009. Gastrointestinal norovirus infection associated with exacerbation of inflammatory bowel disease. J. Pediatr. Gastroenterol. Nutr. **48:**328–333.
21. **Kolykhalov, A. A., S. M. Feinstone, and C. M. Rice.** 1996. Identification of a highly conserved sequence element at the 3′ terminus of hepatitis C virus genome RNA. J. Virol. **70:**3363–3371.
22. **Lai, M. M.** 1998. Cellular factors in the transcription and replication of viral RNA genomes: a parallel to DNA-dependent RNA transcription. Virology **244:**1–12.
23. **Liu, G., Z. Ni, T. Yun, B. Yu, L. Chen, W. Zhao, J. Hua, and J. Chen.** 2008. A DNA-launched reverse genetics system for rabbit hemorrhagic disease virus reveals that the VP2 protein is not essential for virus infectivity. J. Gen. Virol. **89:**3080–3085.
24. **Lowman, H. B., and D. E. Draper.** 1986. On the recognition of helical RNA by cobra venom V1 nuclease. J. Biol. Chem. **261:**5396–5403.
25. **Makeyev, A. V., and S. A. Liebhaber.** 2002. The poly(C)-binding proteins: a multiplicity of functions and a search for mechanisms. RNA **8:**265–278.
26. **Moore, P. B.** 1999. Structural motifs in RNA. Annu. Rev. Biochem. **68:**287–300.
27. **Munder, M., B. S. Choi, M. Rogers, and P. Kropf.** 2009. L-Arginine deprivation impairs Leishmania major-specific T-cell responses. Eur. J. Immunol. **39:**2161–2172.
28. **Ochs, K., A. Zeller, L. Saleh, G. Bassili, Y. Song, A. Sonntag, and M. Niepmann.** 2003. Impaired binding of standard initiation factors mediates poliovirus translation attenuation. J. Virol. **77:**115–122.
29. **Paul, A. V., E. Rieder, D. W. Kim, J. H. van Boom, and E. Wimmer.** 2000. Identification of an RNA hairpin in poliovirus RNA that serves as the primary template in the in vitro uridylylation of VPg. J. Virol. **74:**10359–10370.
30. **Rodriguez Pulido, M., F. Sobrino, B. Borrego, and M. Saiz.** 2009. Attenuated

foot-and-mouth disease virus RNA carrying a deletion in the 3′ noncoding region can elicit immunity in swine. J. Virol. **83:**3475–3485.

31. **Said, M. A., T. M. Perl, and C. L. Sears.** 2008. Healthcare epidemiology: gastrointestinal flu: norovirus in health care and long-term care facilities. Clin. Infect. Dis. **47:**1202–1208.

32. **Sandoval-Jaime, C., and A. Gutiérrez-Escolano.** 2009. Cellular proteins mediate 5′-3′ end contacts of Norwalk virus genomic RNA. Virology **387:**322.

33. **Sawicka, K., M. Bushell, K. A. Spriggs, and A. E. Willis.** 2008. Polypyrimidine-tract-binding protein: a multifunctional RNA-binding protein. Biochem. Soc. Trans. **36:**641–647.

34. **Siebenga, J. J., H. Vennema, D. P. Zheng, J. Vinje, B. E. Lee, X. L. Pang, E. C. Ho, W. Lim, A. Choudekar, S. Broor, T. Halperin, N. B. Rasool, J. Hewitt, G. E. Greening, M. Jin, Z. J. Duan, Y. Lucero, M. O'Ryan, M. Hoehne, E. Schreier, R. M. Ratcliff, P. A. White, N. Iritani, G. Reuter, and M. Koopmans.** 2009. Norovirus illness is a global problem: emergence and spread Of norovirus GII.4 variants, 2001–2007. J. Infect. Dis. **200:**802–812.

35. **Simmonds, P., I. Karakasiliotis, D. Bailey, Y. Chaudhry, D. J. Evans, and I. G. Goodfellow.** 2008. Bioinformatic and functional analysis of RNA secondary structure elements among different genera of human and animal caliciviruses. Nucleic Acids Res. **36:**2530–2546.

36. **Sosnovtsev, S. V., G. Belliot, K.-O. Chang, O. Onwudiwe, and K. Y. Green.** 2005. Feline calicivirus VP2 is essential for the production of infectious virions. J. Virol. **79:**4012–4024.

37. **Sosnovtsev, S. V., G. Belliot, K.-O. K. Chang, V. G. Prikhodko, L. B. Thackray, C. E. Wobus, S. M. Karst, H. W. Virgin, and K. Y. Green.** 2006. Cleavage map and proteolytic processing of the murine norovirus nonstructural polyprotein in infected cells. J. Virol. **80:**7816–7831.

38. **Straub, T. M., K. H. Z. Bentrup, P. Orosz-Coghlan, A. Dohnalkova, B. K. Mayer, R. A. Bartholomew, C. O. Valdez, C. J. Bruckner-Lea, C. P. Gerba, M. Abbaszadegan, and C. A. Nickerson.** 2007. In vitro cell culture infectivity assay for human noroviruses. Emerg. Infect. Dis. **13:**396–403.

39. **Tanaka, T., N. Kato, M. J. Cho, and K. Shimotohno.** 1995. A novel sequence found at the 3′ terminus of hepatitis C virus genome. Biochem. Biophys. Res. Commun. **215:**744–749.

40. **Thackray, L. B., C. E. Wobus, K. A. Chachu, B. Liu, E. R. Alegre, K. S. Henderson, S. T. Kelley, and H. W. T. Virgin.** 2007. Murine noroviruses comprising a single genogroup exhibit biological diversity despite limited sequence divergence. J. Virol. **81:**10460–10473.

41. **Turcios-Ruiz, R. M., P. Axelrod, K. St. John, E. Bullitt, J. Donahue, N. Robinson, and H. E. Friss.** 2008. Outbreak of necrotizing enterocolitis caused by norovirus in a neonatal intensive care unit. J. Pediatr. **153:**339–344.

42. **Vashist, S., D. Bailey, A. Putics, and I. Goodfellow.** 2009. Model systems for the study of human norovirus biology. Future Virol. **4:**353–367.

43. **Wang, H., X. T. Shen, R. Ye, S. Y. Lan, L. Xiang, and Z. H. Yuan.** 2005. Roles of the polypyrimidine tract and 3′ noncoding region of hepatitis C virus RNA in the internal ribosome entry site-mediated translation. Arch. Virol. **150:**1085–1099.

44. **Ward, V. K., C. J. McCormick, I. N. Clarke, O. Salim, C. E. Wobus, L. B. Thackray, H. W. T. Virgin, and P. R. Lambden.** 2007. Recovery of infectious murine norovirus using pol II-driven expression of full-length cDNA. Proc. Natl. Acad. Sci. USA **104:**11050–11055.

45. **Yamada, N., K. Tanihara, A. Takada, T. Yorihuzi, M. Tsutsumi, H. Shimomura, T. Tsuji, and T. Date.** 1996. Genetic organization and diversity of the 3′ noncoding region of the hepatitis C virus genome. Virology **223:**255–261.

46. **Yanagi, M., M. St. Claire, S. U. Emerson, R. H. Purcell, and J. Bukh.** 1999. In vivo analysis of the 3′ untranslated region of the hepatitis C virus after in vitro mutagenesis of an infectious cDNA clone. Proc. Natl. Acad. Sci. USA **96:**2291–2295.

47. **Yu, L., J. R. Putnak, A. G. Pletnev, and L. Markoff.** 2008. Attenuated West Nile viruses bearing 3′SL and envelope gene substitution mutations. Vaccine **26:**5981.

48. **Zuker, M.** 1989. On finding all suboptimal foldings of an RNA molecule. Science **244:**48–52.